

Regional environmental change versus local signal preservation in Holocene thermokarst lake sediments: A case study from Herschel Island, Yukon (Canada)

Michael Fritz  · Ingmar Unkel  · Josefine Lenz  · Konrad Gajewski  ·
Peter Frenzel · Nathalie Paquette · Hugues Lantuit  · Lisa Körte ·
Sebastian Wetterich 

Received: 14 December 2015 / Accepted: 5 March 2018 / Published online: 15 March 2018
© Springer Science+Business Media B.V., part of Springer Nature 2018

Abstract Thermokarst lakes cover nearly one fourth of ice-rich permafrost lowlands in the Arctic. Sediments from an athalassic subsaline thermokarst lake on Herschel Island (69°36'N; 139°04'W, Canadian Arctic) were used to understand regional changes in climate and in sediment transport, hydrology, nutrient availability and permafrost disturbance. The sediment record spans the last ~ 11,700 years and the basal date is in good agreement with the Holocene onset of thermokarst initiation in the region. Electrical

conductivity in pore water continuously decreases, thus indicating desalinization and continuous increase of lake size and water level. The inc/coh ratio of XRF scans provides a high-resolution organic-carbon proxy which correlates with TOC measurements. XRF-derived Mn/Fe ratios indicate aerobic versus anaerobic conditions which moderate the preservation potential of organic matter in lake sediments. The coexistence of marine, brackish and freshwater ostracods and foraminifera is explained by (1) oligohaline to mesohaline water chemistry of the past lake and (2) redeposition of Pleistocene specimens found within upthrust marine sediments around the lake. Episodes of catchment disturbance are identified when

Electronic supplementary material The online version of this article (<https://doi.org/10.1007/s10933-018-0025-0>) contains supplementary material, which is available to authorized users.

M. Fritz (✉) · J. Lenz · H. Lantuit · S. Wetterich
Department of Periglacial Research, Alfred Wegener
Institute Helmholtz Center for Polar and Marine Research,
Potsdam, Germany
e-mail: michael.fritz@awi.de

J. Lenz
e-mail: josefine.lenz@awi.de

H. Lantuit
e-mail: hugues.lantuit@awi.de

S. Wetterich
e-mail: sebastian.wetterich@awi.de

I. Unkel · L. Körte
Institute for Ecosystem Research, Christian-Albrechts-
Universität zu Kiel, Kiel, Germany
e-mail: iunkel@ecology.uni-kiel.de

L. Körte
e-mail: lisa_koerte@gmx.de

J. Lenz · H. Lantuit
Institute of Earth and Environmental Sciences, University
of Potsdam, Potsdam, Germany

K. Gajewski · N. Paquette
Laboratory for Paleoclimatology and Climatology,
Department of Geography, Environment and Geomatics,
University of Ottawa, Ottawa, Canada
e-mail: gajewski@uottawa.ca

N. Paquette
e-mail: npaqu057@gmail.com

P. Frenzel
Institute of Earth Sciences, Friedrich Schiller University
of Jena, Jena, Germany
e-mail: peter.frenzel@uni-jena.de

calcareous fossils and allochthonous material were transported into the lake by thermokarst processes such as active-layer detachments, slumping and erosion of ice-rich shores. The pollen record does not show major variations and the pollen-based climate record does not match well with other summer air temperature reconstructions from this region. Local vegetation patterns in small catchments are strongly linked to morphology and sub-surface permafrost conditions rather than to climate. Multidisciplinary studies can identify the onset and life cycle of thermokarst lakes as they play a crucial role in Arctic freshwater ecosystems and in the global carbon cycle of the past, present and future.

Keywords Arctic · Permafrost · Athalassic subsaline lake · XRF scanning · Pore-water hydrochemistry · Ostracoda

Introduction

Thermokarst lakes cover nearly 25% of the ice-rich permafrost lowlands of Arctic Canada (Marsh et al. 2009), Alaska (Hinkel et al. 2005) and Siberia (Grosse et al. 2005). For example, on the Arctic Coastal Plain of northern Alaska, thermokarst lakes presently occupy 22.5% of the surface area, and drained thermokarst lake basins occupy 61.8% (Jones and Arp 2015). Thermokarst lakes form when thaw and ground-ice melt lead to ground subsidence. Precipitation and gravitational subsurface flow let water pool in an initial depression where vertical drainage is inhibited by the permafrost. The resulting lakes are usually shallow (< 5 m), sometimes oriented and rapidly changing in terms of size, water level, and sediment input.

Walter Anthony et al. (2014) documented the large quantities of organic carbon (up to 159 ± 24 Pg C) stored in thermokarst lake basins of Holocene age in the Yedoma region. As the terrestrial Arctic warms, permafrost soils, including those located in drained lake basins, are expected to release substantial greenhouse gas emissions that will generate a positive feedback to global warming (Dutta et al. 2006; Koven et al. 2011; Schaefer et al. 2014). Walter Anthony et al. (2014) indicated that widespread permafrost thaw could ultimately result in reduced lake and wetland

abundance caused by drainage and drying, facilitating rapid organic carbon decomposition.

Thermokarst lakes in Arctic tundra landscapes are dynamic features with highly variable timing in terms of life cycle (Burn and Smith 1990; Hinkel et al. 2003; Lenz et al. 2016) that includes initiation, expansion, drainage and eventual re-initiation (Mackay 1988; van Huissteden et al. 2011). The initiation of thermokarst lakes in northwest Canada, Alaska, and Siberia is related to increasing air temperatures, available moisture and permafrost thaw in response to warming during the late glacial period and following Pleistocene-Holocene transition (Rampton 1988; Walter Anthony et al. 2014). In Northwest Canada, the waning Laurentide Ice Sheet resulted in a general extensive reorganization of landscapes (Kaufman and Manley 2004). Rapid environmental change included thermokarst lake development which peaked during the Holocene Thermal Maximum (HTM), a post-glacial warm period with warmer-than-modern summer air temperatures. The spatio-temporal pattern of the HTM was asymmetric across the Arctic with Alaska and northwest Canada experiencing warming about 4000 years earlier than northeast Canada and Greenland which were affected by cooling of the residual Laurentide Ice Sheet (Kaufman et al. 2004). Warmer conditions in the Yukon and Northwest Territories are indicated from pollen and macrofossil records which reconstructed a northward expansion of the tree line and thermophilic plants like *Myrica*, *Typha* and *Populus* between 11,600 and 5600 years (Cwynar 1982; Ritchie et al. 1983; Cwynar and Spear 1991; Spear 1993). Active layer deepening and thaw subsidence due to intense ground-ice melt out (Burn et al. 1986; Burn 1997) as well as the formation of thermokarst lakes peaked between 11,600 and 10,300 year BP (Rampton 1988; Murton 2001; Dallimore et al. 2000). However, Kaufman et al. (2016) concluded from a systematic proxy review that air temperatures were highly variable in Alaska and western Canada. In this context, thermokarst lakes provide valuable paleoenvironmental information preserved in the sedimentary, geochemical and paleontological properties of lacustrine deposits. Because the aggradation and degradation of permafrost are controlled by both large-scale climate variations and local conditions such as vegetation, substrate, precipitation and hydrology, the paleoenvironmental information preserved in permafrost deposits is biased by

interrelated processes and dependencies. The use of thermokarst deposits in paleoenvironmental research, therefore, needs a clear understanding of signal sources and careful interpretation.

The goal of this study is to show that thermokarst lake sediment records are valuable environmental archives in permafrost landscapes that capture large-scale climate variations and local landscape changes. We seek to provide a better understanding on which environmental proxies reflect large-scale changes in climate and which are more related to local changes in sediment transport, hydrology, nutrient availability and surface disturbance. The specific objectives of this manuscript are:

1. to show that episodic permafrost disturbance in the catchment leaves an imprint in the sedimentological record of thermokarst lakes,
2. to relate and reconstruct the chemical development of an athalassic subsaline lake; the changes in lake-water hydrochemistry and sediment-input patterns to changing habitat conditions for calcareous microfossil taxa,
3. to assess the ability of different proxies to provide quantitative climate reconstructions in thermokarst settings, and to distinguish between climatically-relevant information on large scales and local conditions.

Study site

This study combines sedimentological data, pore-water hydrochemistry and paleontological proxy data, such as pollen and ostracods from a Holocene thermokarst lake core from Herschel Island (69°36'N; 139°04'W) in the northern Yukon, Canada. Herschel Island in the Southern Beaufort Sea is part of the Yukon Coastal Plain in the western Canadian Arctic (Fig. 1). The modern climate of northernmost Yukon is subarctic maritime in summer during the open-water season, and continental in winter (Wahl et al. 1987). The mean annual air temperature (1971–2000) is $-11\text{ }^{\circ}\text{C}$ at Komakuk Beach, the closest weather station $\sim 40\text{ km}$ west of Herschel Island, with an average July maximum of $7.8\text{ }^{\circ}\text{C}$ (Environment Canada 2015). Mean total annual precipitation is between 161 mm year^{-1} at Komakuk Beach and 254 mm year^{-1} at Shingle Point ($\sim 100\text{ km}$ southeast of Herschel Island) and is

almost equally divided between rain and snow (Environment Canada 2015). The typical vegetation of Herschel Island is tussock tundra dominated by grasses, herbs, dwarf shrubs and various mosses and lichens (Smith et al. 1989). Herschel Island is primarily composed of marine sands, silts and silty clays with incorporated carbonate fossils from the continental shelf as it was formed as a Pleistocene push moraine that emerged from the last regional advance of the Laurentide Ice Sheet (Mackay 1959) between around 20,000 cal BP (Zazula et al. 2009) and 16,000 cal BP (Fritz et al. 2012a, b). Today, Herschel Island reaches the highest elevation along the Yukon Coastal Plain with 183 m a.s.l. (meter above sea level) whereas the carved out Herschel Basin southeast of Herschel Island reaches depths of about 70 m below sea level (Mackay 1959; Fig. 1). The island is characterized by continuous, ice-rich permafrost with up to 70% ground ice content in the upper 10–15 m occurring as segregated ice lenses, ice wedges, pore ice, and massive tabular ice bodies in the form of buried glacier ice, snow bank ice, and massive segregated ice (Fritz et al. 2011, 2012b). Polygonal patterned ground and ponds have formed in flat areas since deglaciation (Fritz et al. 2016).

A large thermokarst lake (informal name: Lake Herschel), located in the center of Herschel Island (69°36'03"N, 139°03'47"W), is about 400 m in diameter, 0.126 km^2 in area and up to 6 m deep (Lenz et al. 2013; Fig. 1). The lake circulation is cold-monomictic. The water body is mixed in summer with a water temperature of $\sim 8\text{ }^{\circ}\text{C}$, electrical conductivity (EC) of 1.1 mS cm^{-1} and a pH of 7.2–8.3. Under the winter ice cover of 2 m the EC of lake water increased to 2.3 mS cm^{-1} and water temperatures of about $1\text{ }^{\circ}\text{C}$ were measured (Lenz et al. 2013).

Materials and methods

Sediment core

The sedimentological and biogeochemical properties of the 727-cm-long lake sediment core (core ID: PG1967) of Lake Herschel were described in detail by Lenz et al. (2013) and are summarized in Electronic Supplementary Material (ESM 1). Four sedimentary units were distinguished which resembled the four phases of lake development during the Holocene by

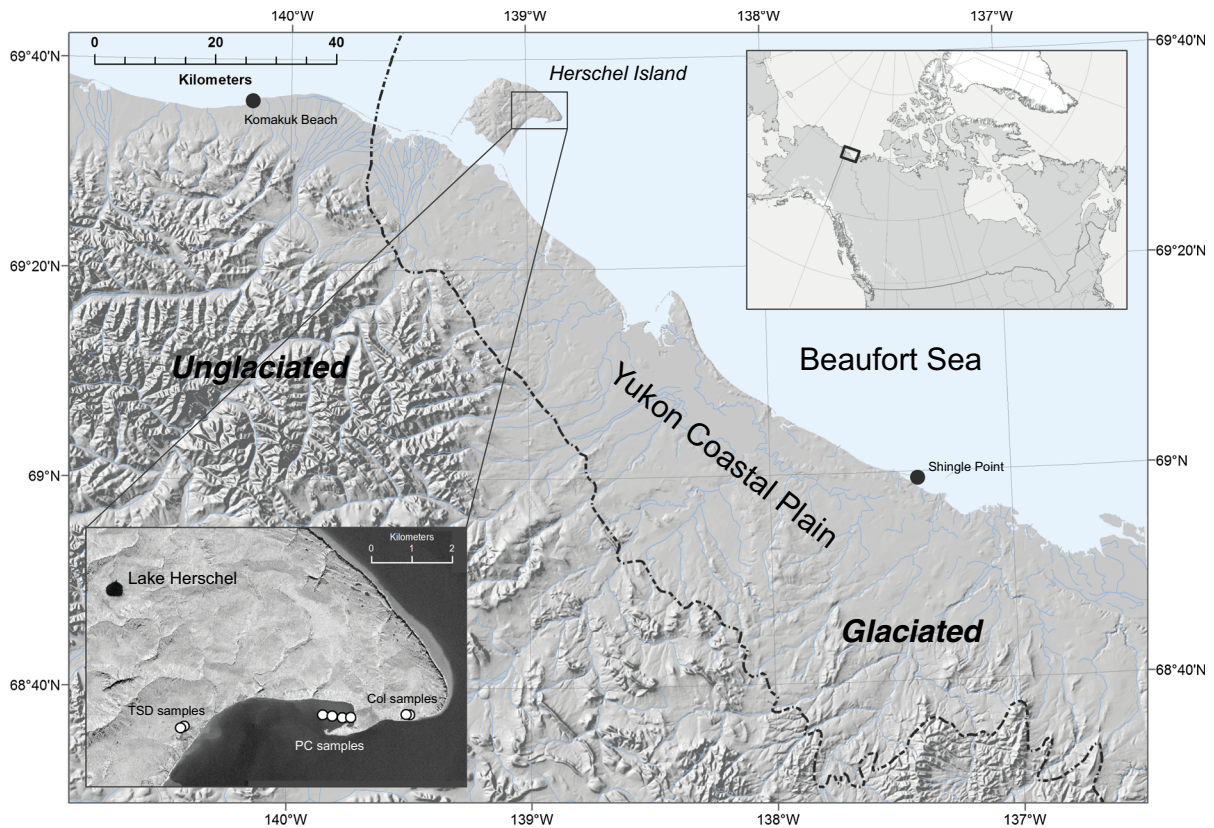


Fig. 1 Map of the study area showing location of Lake Herschel on Herschel Island in the western Canadian Arctic (Ikonos image 2001). Detailed map (lower left inset) shows location of Lake Herschel and fossil reference samples from

Colinson Head (Col samples) and samples from Thaw Slump D (TSD samples) as well as modern marine reference samples from Pauline Cove (PC samples)

variations in grain size, biogeochemical parameters, density, water content, and magnetic susceptibility: unit A (727–700 cm), unit B (700–600 cm), unit C (600–207 cm) and unit D (198–0 cm). The clayish to sandy matrix contained bedding structures and, in places, organic layers. Total organic carbon (TOC) content varied between about 2 and 9 wt%, and total nitrogen between about < 0.1 and 0.4 wt%. Largest variations were observed within the early Holocene unit B. Calcium carbonate was present throughout the core. The radiocarbon-based core chronology of Lenz et al. (2013), which is re-evaluated in this study, included eight dates and the age-depth relationship used a quadratic regression model for unit A to C, assuming continuous sedimentation between < 11,500 and 1800 cal BP and excluding the hiatus between units C and D. Unit D was dated to between 900 cal BP and the present (Lenz et al. 2013).

Radiocarbon dating and age modelling

Nine samples of plant material (mosses, sedges, and wood fragments) and one bivalve mollusk sample were recovered from the core and measured for radiocarbon (^{14}C AMS) ages (ESM 2) at the Poznan Radiocarbon Laboratory, Poland. All ^{14}C samples were calibrated with respect to IntCal13 (Reimer et al. 2013). An age-depth-model was calculated using the OxCal 4.2.3 calibration software (Bronk Ramsey 2009a). This software combines the probability distributions of the calibrated radiocarbon ages with certain assumptions on depositional processes to obtain an age-depth-curve with 1σ (68.2%) probability margins of the radiocarbon ages. We applied the *P_Sequence* model of OxCal 4.2.3 to our data which assumes the deposition to be random (meaning no regular annual layers), although with an approximate proportionality to depth z (Bronk Ramsey 2008). We

adopted a k -value of 150, which gives an estimate of the variation from a constant sedimentation rate equivalent to 7-mm calculation increments. An age-depth curve was directly extracted from the OxCal model, returning maximal and minimal ages for every centimeter (Fig. 2). For plotting our proxy data, a curve based on the mean age values was then extracted from OxCal and interpolated to 2 and 5 mm steps using the *interpol*-function (method “linear”) of R version 3.1.2 (R Core Team 2014). Calibrated years are denoted as *cal BP* (i.e. before AD 1950) (Mook and van der Plicht 1999). Outlier ^{14}C dates that differed significantly from the general age-depth-model were assessed using the *Outlier* “charcoal” model of OxCal (Bronk Ramsey 2009b). Outliers were excluded from the calculation of the age-depth-curve if no agreement with the model could be achieved.

Pore-water chemistry

Pore water was obtained using rhizon soil moisture samplers (Rhizon SMS, Eijkelkamp) which have mean pore size of 0.15 μm . Hydrochemical characterization included pH, electrical conductivity (EC), major anions and cations. The cation content was analyzed by inductively coupled plasma-optical emission spectrometry (ICP-OES, Perkin-Elmer Optima 3000 XL), while the anion content was determined by ion chromatography (IC, Dionex DX-320). Hydrogen carbonate concentrations were measured by titration with 0.01 M HCl using an automatic titrator (Metrohm 794 Basic Titrimo). Not every parameter was measured continuously down-core because of sample volume restrictions. Where measurements gave values below the detection limit, we display half of the detection limit. This was sometimes the case for Fe (throughout the core), NO_3 (in units A–C), Ba (in unit D), Mn (in units B and D).

X-ray fluorescence (XRF) scanning

XRF scanning was carried out at a resolution of 2 mm until 290 cm core depth and thereafter at a resolution of 5 mm until 727 cm. The XRF scans were performed at Cologne University (Germany) using an ITRAX core scanner with a molybdenum X-ray source (Croudace et al. 2006). The XRF-scanning results represent element intensities in “counts per second” (cps) which are proportional to chemical concentrations but depend also on sediment properties (Röhl and

Abrams 2000), water content (Tjallingii et al. 2007), and element–element interaction (matrix effect) during measurement (Weltje and Tjallingii 2008). We report the XRF-scanning results as log-ratios to avoid statistical analysis of data sensitive to the closed-sum effect (dilution by organic material) (Weltje and Tjallingii 2008; Löwemark et al. 2011).

Micropaleontology

Calcareous microfossils (ostracods, foraminifers, mollusks)

The micropaleontological material comprised 77 samples from core PG 1967. For comparing the lacustrine record with modern and Pleistocene faunas six additional recent surface sediment samples (four littoral marine and two from Lake Herschel) and four samples from strata from Pleistocene permafrost outcrops with an age of more than 16,000 cal BP, according to Fritz et al. (2012b), were analyzed (Fig. 1). Sediments were washed through a 63 μm sieve, air-dried and picked for ostracods, foraminifers and mollusks as well as other microfossils of the sand-sized fraction under a stereomicroscope. Specimens were identified and their number counted if rare or estimated if highly abundant to produce semi-quantitative abundance data for each group. For revealing factors influencing the distribution of microfossils and for comparing core samples with reference material, a principal component analysis (PCA) based on abundance data was applied using the program package PAST (Hammer et al. 2001).

Palynology

Two cm^3 of sediment were processed to concentrate the pollen from the sediment using standard chemical treatment with the addition of heavy liquid separation (Zabenskie et al. 2006; Zabenskie and Gajewski 2007) and mounted in silicone oil. Tablets of *Lycopodium* were added to the samples prior to treatment to enable the computation of pollen concentrations, and these were multiplied by the sedimentation rate to provide estimates of influx ($\text{grains cm}^{-2} \text{ year}^{-1}$). Pollen counting was difficult due to low concentrations and the presence of many poorly preserved grains; an average of 270 grains were counted per interval, with the range from 237 to 312 grains. Paleoclimate

estimates were based on the modern analogue technique (MAT) and modern pollen samples from the North America Modern Pollen Database (Whitmore et al. 2005; Williams et al. 2006). The squared chord distance (SCD) was used as the dissimilarity measure. Only samples from the tundra and forest-tundra in the modern database were retained as possible analogues; for the climate reconstruction our pollen sum consisted of 26 NAP taxa (ESM 3).

Results

Data presented in this work are available from the PANGAEA database at <https://doi.pangaea.de/10.1594/PANGAEA.886875> (Fritz et al. 2018). Supplementary figures are available in the electronic supplementary material (ESM) to this article.

Chronostratigraphy: the revised age model

The age-depth model (Fig. 2) shows continuous sedimentation from the core bottom until a depth of 197 cm, which covers the period from 11,670 to 1590 cal BP. The bivalve sample (*Pisidium* sp., Poz-36423) taken at 57–61 cm shows an apparent age of 920 ± 40 ^{14}C years. However, individuals living at the lake bottom included a substantial amount of dead carbon in their carbonate shell and therefore this date was excluded from the age-depth model. Two ^{14}C dates (Poz-36426, 36427, ESM 2) obtained at 366 and 528 cm depth were also identified as outliers and excluded. The respective plant material was probably eroded from the catchment and transported into the lake by water or ice. Two ^{14}C dates were obtained immediately below and above a distinct light-gray sandy layer of coarser grain size at 207 and 198 cm

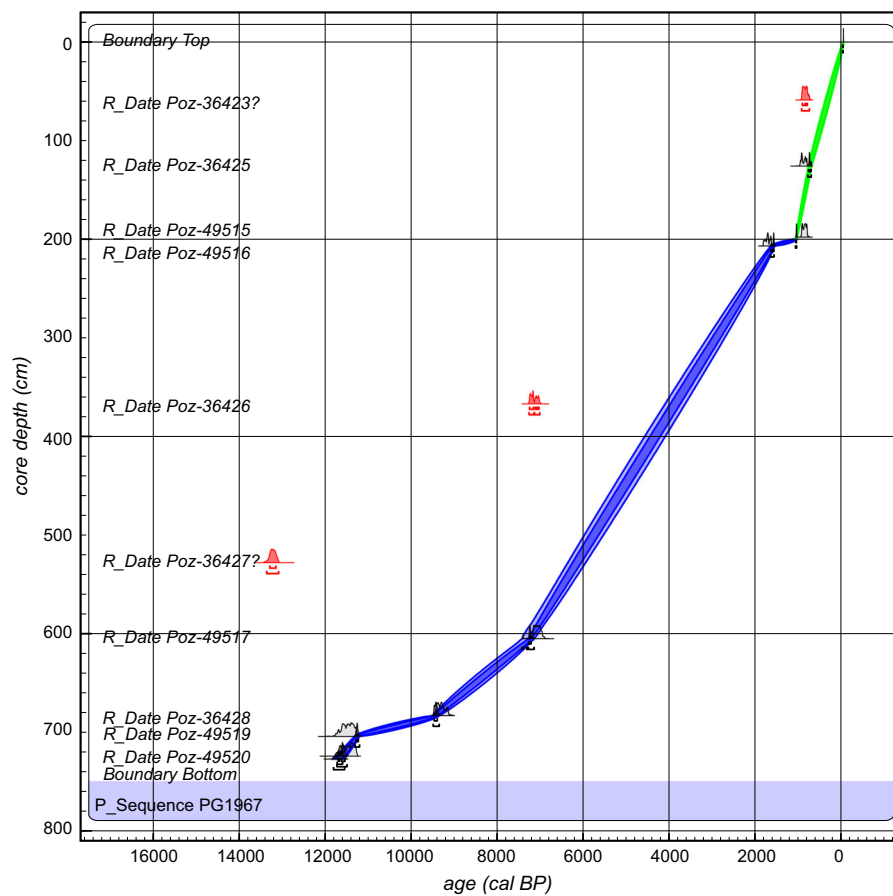


Fig. 2 Age-depth-model of core PG1967 from Lake Herschel calculated and plotted using the software OxCal 4.2.3 (Bronk Ramsey 2009a). Blue lines are used for the age-depth-range

before the hiatus, green lines for the range after the hiatus. The inner ranges reflect 1 σ (68.2%) probability ranges, the outer ranges 2 σ (95.4%) probability. Outliers are marked in red

depth, respectively (Poz-49515, 49516, ESM 2). These two dates, only 9 cm apart, have mean ages of 1590 and 1040 cal BP respectively, with a minimum distance of their 1- σ ranges of 490 years. It is not clear at what point of time the sandy layer between these dates was deposited, but the ^{14}C ages support a chronological hiatus between them. Based on this age model we consider the sediment units to represent the following periods:

- unit A (727–700 cm; > 11,660–10,930 cal BP);
- unit B (700–600 cm; ~ 10,930–7170 cal BP);
- unit C (600–207 cm; ~ 7170–1590 cal BP);
- hiatus (1590 cal BP to 1040 cal BP; approximately 550 years);
- unit D (198–0 cm; 1040 cal BP to 2009 AD).

The deposition periods of the sediment units (A–D) of the Lake Herschel core PG1967 previously established by Lenz et al. (2013) are for the most part confirmed by the refined age model presented here. Differences occur due to application of the updated calibration data set by Reimer et al. (2013) and the newly applied age modelling as described above.

XRF chemistry

We here focus on four selected element ratios which are most suitable for comparison with the other proxies reported in this study: (1) the incoherent (inc) and coherent (coh) electron scattering which is recorded by ITRAX XRF scanners in addition to the element counts; (2) the Mn/Fe ratio (Fig. 3) providing information on redox conditions and alkalinity and thus on preservation conditions for organic matter; (3) the Sr/Ca ratio (Fig. 4) which changes in carbonate shells in reaction to changes in lake-water salinity (Ricketts et al. 2001), and (4) the Rb/Sr ratio which is an indicator for weathering in the catchment and is sensitive to temperature variations (Jin et al. 2001).

Inc/coh ratio and total organic carbon (TOC)

Incoherent scattering is higher for elements with low atomic mass like carbon. Hence, the ratio of incoherent to coherent (inc/coh) scattering can be used as an indicator of the organic carbon content (Guyard et al. 2007; Burnett et al. 2011; Chawchai et al. 2016). Here, the inc/coh ratio correlates well with measurements of TOC ($r = 0.42$, $p < 0.001$), and therefore provides a

high-resolution proxy for organic carbon content in comparison to the TOC measurements performed at coarser resolution (Fig. 3). The inc/coh ratio was lowest at the very bottom of the core sequence. It then increased moderately until 11,200 cal BP and more strongly until approx. 11,000 cal BP (Fig. 3). Between 9400 and 8200 cal BP there were three peaks in inc/coh ratio that broadly corresponded to high values in TOC. After 8200 cal BP, inc/coh and TOC never reached the same high values as before. With the onset of unit D (after the sedimentation hiatus) the inc/coh ratio was generally higher than in unit C. Two distinct peaks around 900 cal BP were also reflected in the TOC record.

Manganese/iron (Mn/Fe) ratio

The Mn/Fe ratio was negatively correlated with the inc/coh ratio ($r = -0.37$, $p < 0.001$) and TOC ($r = -0.26$, $p < 0.001$) over the entire sequence, especially notable in Unit B (Fig. 3). A decreasing Mn/Fe ratio (more anaerobic conditions) during unit A was accompanied by increasing inc/coh and TOC, which indicates higher preservation of organic material. While there were no major variations in Mn/Fe or inc/coh in unit C, the “hiatus layer” showed the highest Mn/Fe ratios of the entire sequence, in contrast to minimal TOC. Variations of Fe and Mn in lake sediments are difficult to interpret (Engstrom and Wright 1984) because a number of independent environmental factors control their supply and sedimentation, such as alkalinity and acidity (pH) as well as reduction potential (Eh) (Koinig et al. 2003). Anaerobic conditions and lowered pH favor mobility of iron. As the pH is generally high in our pore-water record (Fig. 5), the Mn/Fe ratio could be regarded as a proxy for aerobic versus anaerobic conditions.

Strontium/calcium (Sr/Ca) ratio

Sr/Ca strongly increased between 11,700 and 10,300 cal BP, only interrupted by a negative peak between 10,800 and 10,300 cal BP (Fig. 4). The Sr/Ca ratio decreased gradually towards 8900 cal BP; this trend was inverted until 8200 cal BP before the ratio decreased again until approximately 6800 cal BP. After 6800 cal BP the Sr/Ca ratio fluctuated around the mean value of the entire sequence before it showed a clear decrease in the “hiatus” layer followed by a

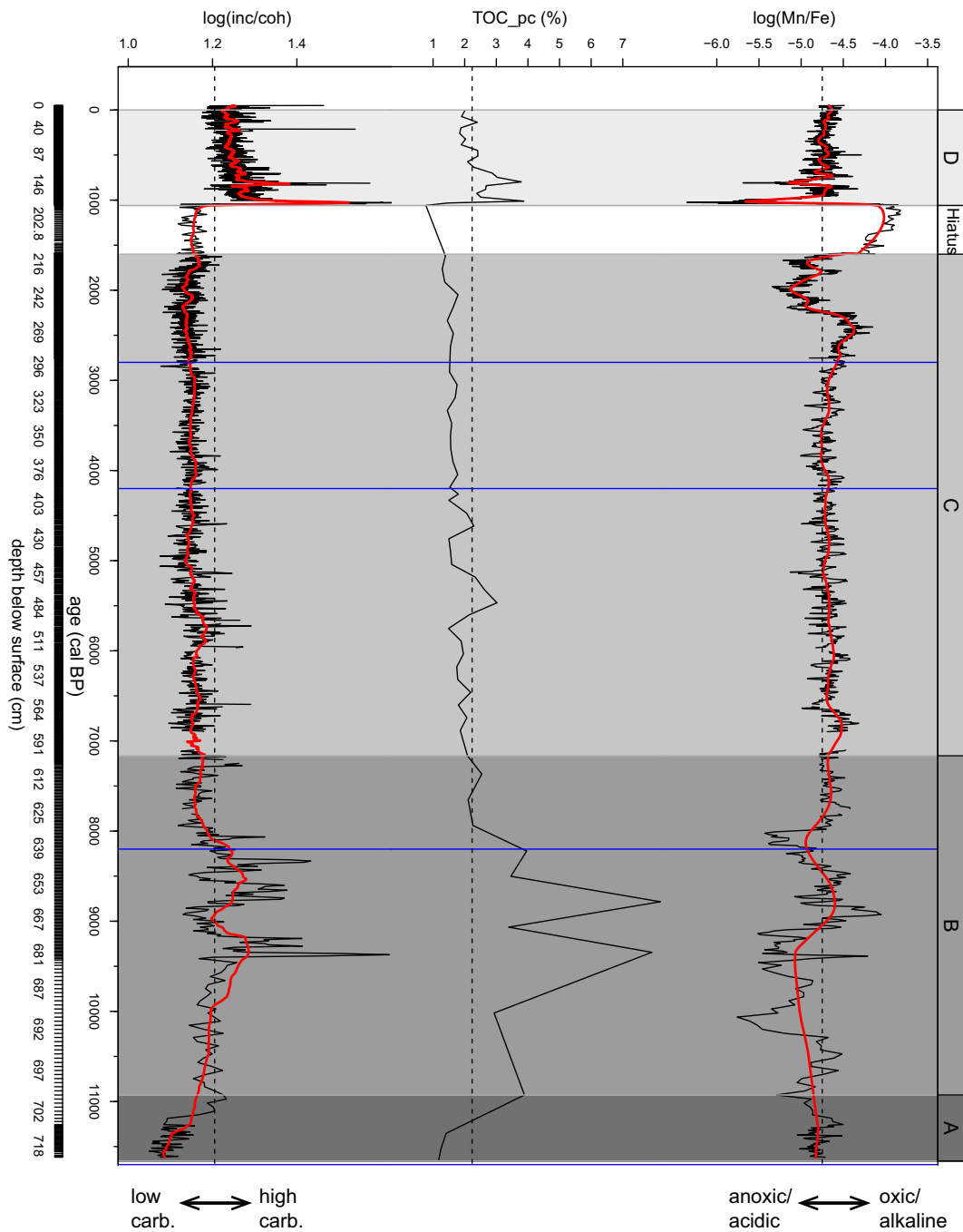


Fig. 3 XRF-based proxy log-ratios (inc/coh, Mn/Fe) compared to absolute TOC measurements from Lake Herschel (TOC taken from Lenz et al. 2013). All proxies plotted against age (cal BP). Measured values plotted in black, red lines for inc/coh and Mn/Fe are a 30pt running mean for visualizing more general trends in the data. Dashed lines indicate the mean value for each proxy

calculated from the entire sequence. Blue lines indicate the approximate time of major Holocene climate events for facilitating comparison: 8.2 ka event (Alley and Ágústsson 2005), 4.2 ka event (Booth et al. 2005) and 2.8 ka event (van Geel et al. 2014)

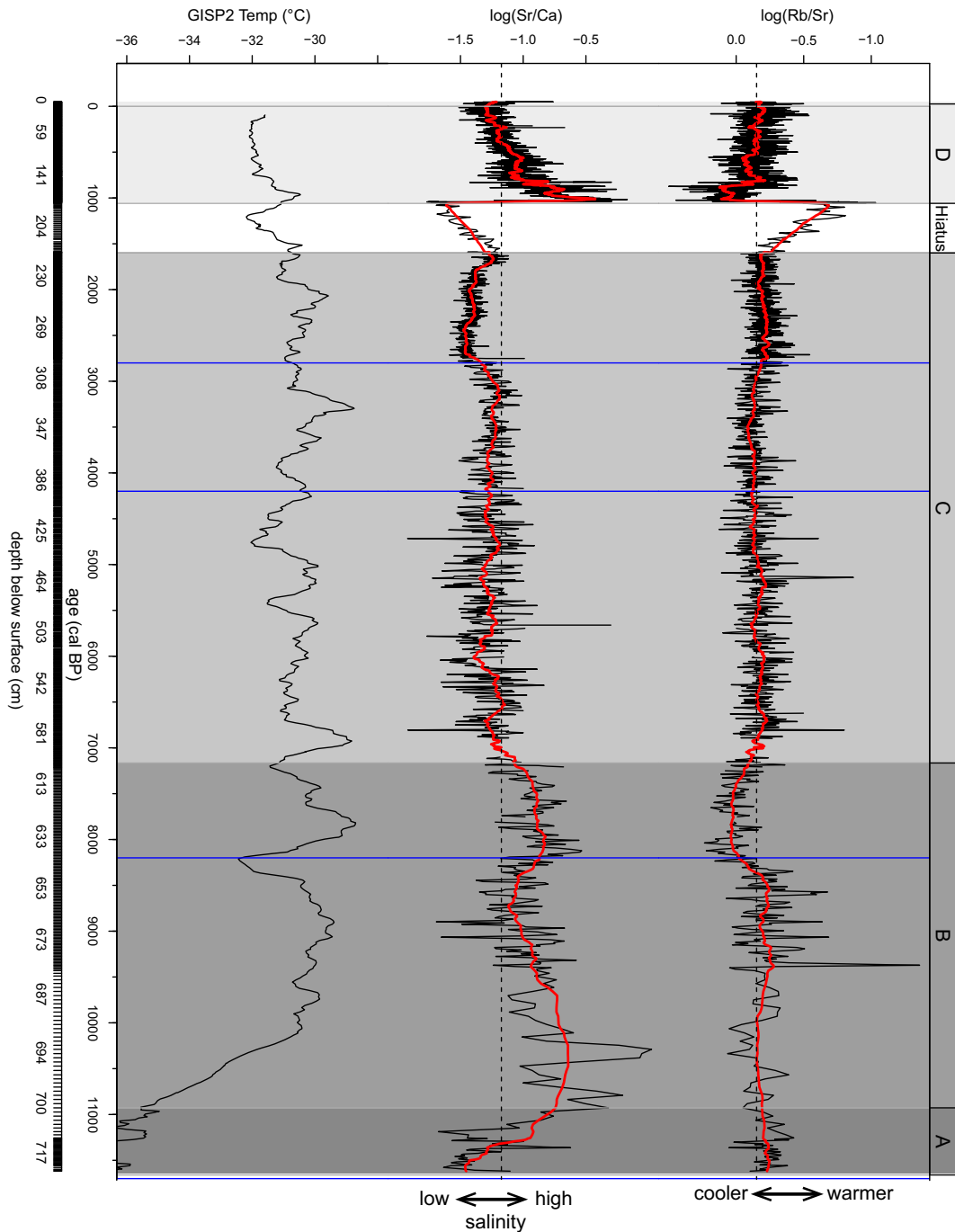


Fig. 4 Greenland GISP2 temperature record for Younger Dryas and Holocene (Alley 2000) compared to XRF-based proxy log-ratios (Sr/Ca) and (Rb/Sr) indicating changes in salinity and temperature, respectively. All proxies plotted against age (cal BP). Measured values plotted in black, red

lines for Sr/Ca and Rb/Sr are a 30pt running mean for visualizing more general trends in the data. Dashed lines indicate the mean value for each proxy calculated from the entire sequence. Blue lines indicate the approximate time of major Holocene climate events (see Fig. 3)

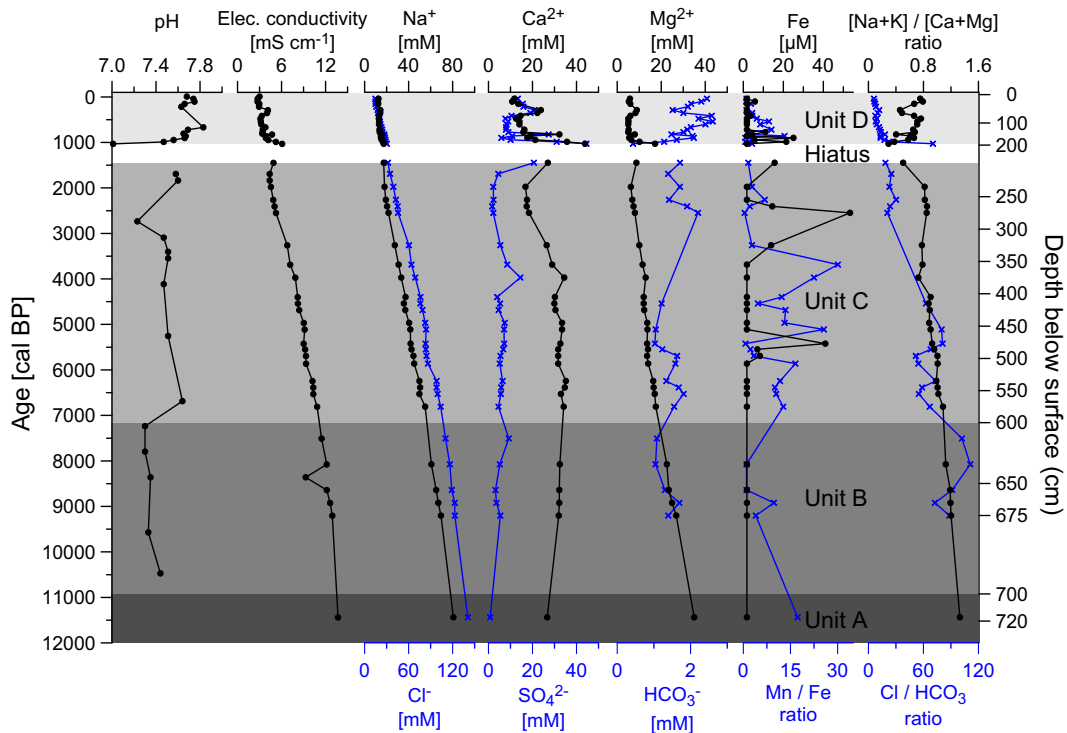


Fig. 5 Pore-water hydrochemistry of Lake Herschel sediments according to age with regard to sedimentary units A–D including the hiatus. Concentrations are displayed in

mol eq. per liter [mM, μ M]. For individual data points see data table in the electronic supplementary material (ESM 6)

sharp rise at the onset of unit D. Strontium (Sr) can substitute for calcium (Ca) in carbonate minerals and co-precipitates in lakes (Cohen 2003). This results in a strong correlation ($r = 0.60\text{--}0.86$, $p < 0.001$) between these two elements (ESM 4). The Sr/Ca ratio of carbonate shells was related to the Sr/Ca ratio of the lake water. While the ratio in ostracod shells seems independent from the temperature of formation it is sensitive to changes in the salinity of the lake water (Mischke et al. 2008; Ricketts et al. 2001).

Rubidium/strontium (Rb/Sr) ratio

The Rb/Sr ratio can be used as a proxy for chemical weathering in the catchment (Jin et al. 2001). High Rb/Sr ratios in lake sediments are related to reduced catchment weathering under cooler climatic conditions, and/or reduced catchment precipitation.

Through most of the sediment sequence the Rb/Sr ratio fluctuated around its mean value (Fig. 4). Only at 8200 cal BP was there a significant shift to a higher

Rb/Sr ratio, indicating a period of cooler conditions which lasted until approximately 7000 cal BP. The strong deviation to a lower Rb/Sr ratio in the “hiatus layer” was most likely not climate-driven.

Pore-water chemistry

Pore water throughout the core was characterized by high EC values between 13.7 and 2.7 mS cm^{-1} (Fig. 5). Lenz et al. (2013) showed modern lake water EC values between 1.1 mS cm^{-1} in summer and 2.3 mS cm^{-1} in winter, which is typical for an athalassic brackish environment in the Arctic (Willemse et al. 2004). A trend of decreasing EC from lake initiation in the early Holocene until about 1600 cal BP is evident. Desalination by increasing freshwater input into the brackish system was interrupted at the hiatus with slightly increasing EC values from 4.4 to 6.0 mS cm^{-1} . The last 1000 years were again characterized by decreasing EC values close to modern bottom lake water characteristics during the winter, although the

modern lake water is chemically dissimilar from the pore water, due to the lower proportion of HCO_3^- in the pore water (ESM 5). The variation in the pore water pH throughout the core was between 7.0 and 7.8. The pH was stable (7.3–7.4) in the early Holocene until 7150 cal BP and more variable and slightly higher (7.2–7.6) until the hiatus at 1590 cal BP. The pH dropped to the overall minimum (7.0) at the hiatus and showed values between 7.5 and 7.8 until today.

Na^+ and Cl^- follow a generally decreasing trend in EC. Na^+ and Cl^- dominated the ion composition with high concentrations until the hiatus at 1590 cal BP, where Ca^{2+} , Mg^{2+} and SO_4^{2-} occurred at maximum concentrations and thus changed the overall ion composition completely (Fig. 5). A decreasing trend in Ca^{2+} concentration is visible between 4000 cal BP and the hiatus at 1590 cal BP, where Ca^{2+} concentrations suddenly rose towards a maximum of 44 mM and then decreased again until today. Fe in measurable concentrations ($> 3.6 \mu\text{M}$) was documented in sediment pore water younger than 5700 cal BP. Mn decreased from 11,500 until 8000 cal BP and then increased, reaching maximum concentrations above 40 μM between 4000 and 3000 cal BP. A decreasing trend in Mn concentrations followed towards the hiatus, where Mn varied strongly and decreased until today. SO_4^{2-} had its minimum (0.8 mM) in the oldest part of the core and remained relatively constant at low levels until the hiatus at 1600 cal BP, where it suddenly reached its maximum concentration of 45 mM. Subsequently, SO_4^{2-} remained at relatively high concentrations with an average value of 15 mM until today. Although we do not have data on HCO_3^- from the oldest core part, a generally increasing trend upwards was detected in the remainder. The HCO_3^- minimum occurred at the hiatus with 0.4 mM. All hydrochemical data is available in the Electronic Supplementary Material (ESM 6).

Calcareous microfossils (ostracods, foraminifers, mollusks)

Reference samples

The four modern marine littoral samples contained the highest number of microfossils. The dominant taxa in these samples are the foraminifers *Haynesina orbiculare* and *Cribolephidium excavatum* and the brackish water ostracods *Heterocyprideis sorbyana*,

Paracyprideis fennica and *Palmoconcha russelensis* (ESM 7). The same species also occurred in the Pleistocene permafrost outcrop samples, although less frequently. Marine or brackish ostracods or foraminifers were completely missing in the two modern Lake Herschel sediment samples. Mollusk fragments were rare and limited to the marine and outcrop samples, sometimes comprising freshwater taxa as well. All microfossil groups encountered within the reference samples (ESM 7) were also found in the core (ESM 8).

Distribution of microfossils in Lake Herschel sediments

Ostracods and foraminifers were present throughout the core, in contrast to the occasional presence of bivalve fragments (Fig. 6). Unit A was characterized by abundant marine to brackish foraminifers and ostracods, including a few marine and a number of freshwater bivalve fragments. Terrestrial microfossils were rare in all samples of the basal unit A. In general, frequencies of occurrence of marine and brackish microfossils were low in unit B with marine mollusks remains in the lower part whereas freshwater ostracods were more abundant than in unit A. The overlying units C to D were characterized by a constant abundance of freshwater ostracods and a varying number of marine to brackish microfossils, with an absence of marine-brackish and brackish ostracods from 5000 to 2000 cal BP (Fig. 6). Marine foraminifers were abundant within unit C but absent from 3500 to 2500 cal BP. In unit D freshwater ostracods and freshwater bivalves showed constant abundance between 10 and 100 specimens, whereas brackish-marine microfossils were less frequently found. The abundance of terrestrial taxa, such as insect remains, oribatid mites and plant remains varied throughout the sediment sequence; they were most abundant in unit D (Fig. 6). Marine mollusks were missing from this part of the core whereas the freshwater bivalve *Pisidium* was quite common. A list of taxa with their main habitats and distribution is given in ESM 8 along with illustrations of selected taxa.

Pollen

There were few changes through time in the pollen assemblages. Pollen of Cyperaceae and Poaceae were the most abundant taxa (Fig. 7); Cyperaceae pollen

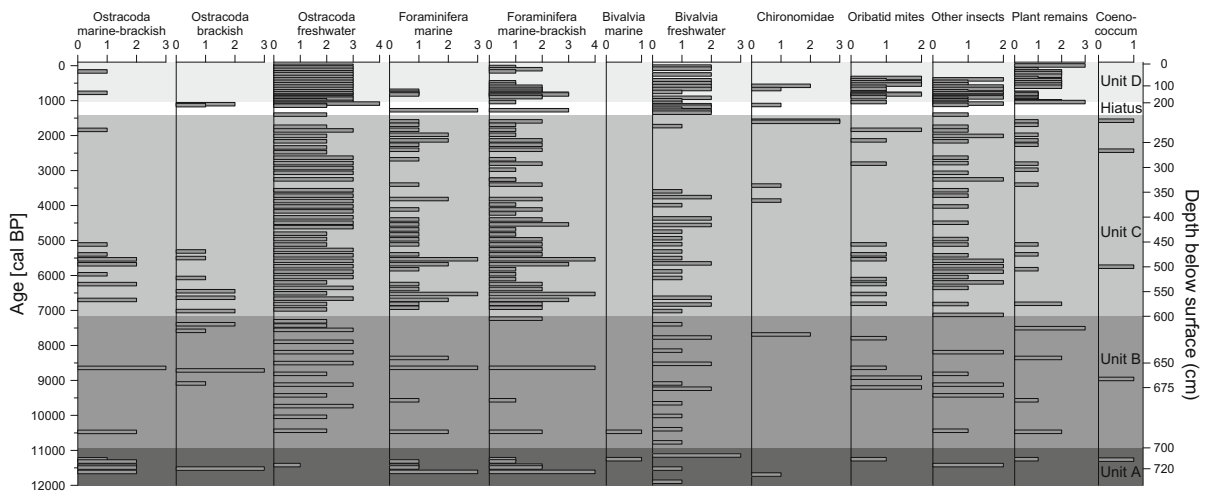


Fig. 6 Semi-quantitative distribution of microfossil groups in sediments from Lake Herschel shown according to age. Abundance classes: 1 = 1–2 specimens; 2 = 3–10 specimens;

3 = 11–100 specimens; 4 = 101–1000 specimens. For a species list see electronic supplementary material (ESM 8)

were more abundant in sediments older than 2000 cal BP (units A–C), and decreased in the past 1000 years. Between 7000 and 2000 cal BP, Cyperaceae percentages were variable but generally high. Poaceae pollen percentages steadily increased between 9000 and 3500 cal BP, and more rapidly in the past 3000 years. Pollen from several shrubs was found in relatively high quantities, including *Alnus*, *Betula* and *Juniperus*. *Salix* pollen percentages were high in the lowermost and also in the uppermost sediments. Tree taxa comprised 3–20% of the total pollen grains, with little change through time (Fig. 7).

Pollen concentrations and influx were low prior to 6000 cal BP. They then increased and remained high, although somewhat variable for the past 5500 years, and total pollen influx was especially high in the past 1000 years. Reconstructed mean July air temperatures varied around present-day values (Komakuk meteorological station, Fig. 1) but were typically below the present-day value during the past 3500 years (Fig. 8). Values of squared chord distance (SCD) were relatively high and changed little through time.

Discussion

Sedimentation history of Lake Herschel

The evolution of Lake Herschel deduced from multi-parameter analyses of the sedimentary record (Lenz

et al. 2013) differentiates four lake stages spanning the Holocene since about 11,700 cal BP. A late Holocene hiatus was identified by radiocarbon dating and sediment properties, and occurred between about 1590 and 1040 cal BP (Lenz et al. 2013).

The lake onset started in response to thermokarst processes between > 11,500 and 10,000 cal BP by melting of massive ground ice and subsequent surface subsidence which shaped the lake's basin. Favorable climate conditions (warmer and wetter than today) during the Holocene thermal maximum from 10,600 to 7000 cal BP in NW Canada (Kaufman et al. 2004; Gajewski 2015a) encouraged lake development. Between about 10,000 and 7000 cal BP, ongoing ground-ice melting deepened the lake to a depth exceeding 2 m so that the water body did not freeze to the bottom in winter, ensuring that a continuously unfrozen zone (talik) developed below the lake. The mid-Holocene lake phase between about 7000 and 1800 cal BP is considered as a dynamic equilibrium of lake development. High sedimentation rates indicate that the lake steadily expanded and that lateral extension of the basin by shore erosion surrounding ice-rich terrain took place. A disturbance in sedimentation is obvious in the late Holocene lake phase between about 1590 and 1040 cal BP. This coincides with the coldest period of the Holocene in the western Arctic (Gajewski 2015a). Two hypotheses to explain the hiatus were outlined by Lenz et al. (2013); either allochthonous slumping disturbed the continuous

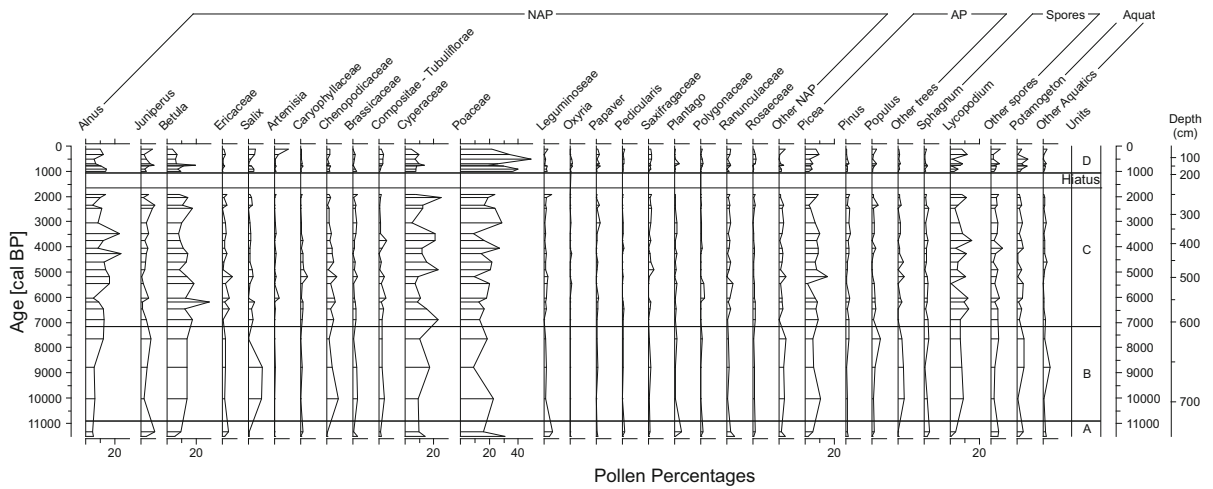


Fig. 7 Percentage pollen diagram from Lake Herschel, Herschel Island, Yukon

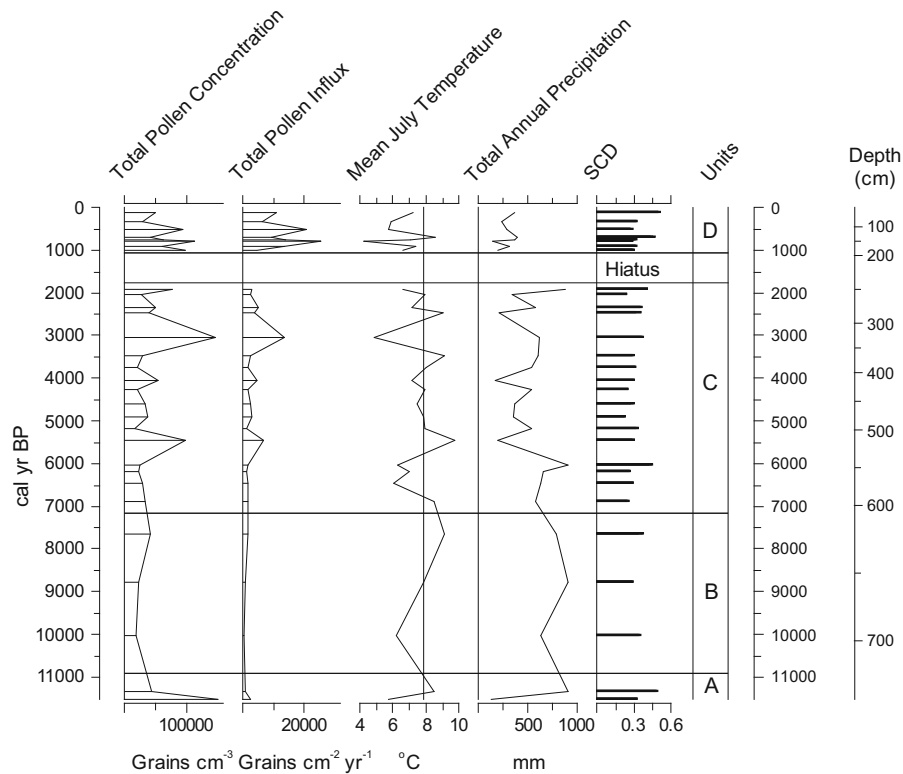


Fig. 8 Total pollen concentration, pollen influx and reconstructed July air temperatures based on the top analogues and squared chord distance (SCD) of the top analogue from Lake

Herschel. The axis of the temperature reconstruction is placed at the mean July air temperature at Komakuk Beach which is 7.8 °C (Environment Canada 2015)

sedimentation or an abrupt lake level fall interrupted the accumulation of lacustrine sediments. After about 1000 cal BP until today the lake is considered to have reached its modern dimensions.

Due to the position and development of Lake Herschel in ice-rich preglacial deposits of marine origin that have undergone ice-thrust deformation (Fritz et al. 2012b), brackish conditions are assumed

and indicated by the inventory of calcareous fossils (foraminifera, mollusks and ostracods) and by XRF geochemistry (Sr/Ca ratio). Lake expansion by degrading marine ice-rich deposits increased the supply of solutes into the evolving lake. This rather uncommon setting requires special attention when interpreting the fossil record of Lake Herschel in terms of paleoecology and paleoclimate.

Limnological, sedimentary and geochemical properties predefine the habitat

Decreasing EC and Sr/Ca ratios from the lake initiation in the early Holocene until about 1600 cal BP indicates desalinization, which points to a lake-level rise with increasing freshwater input. A trend towards freshwater conditions is supported by decreasing $[\text{Na} + \text{K}]/[\text{Ca} + \text{Mg}]$ and Cl/HCO_3^- ratios in the pore water (Fig. 5). However, the general salinity was always and still is elevated compared to typical Arctic freshwaters. Lake Herschel as an athalassic subsaline lake represents a lake type that has been rarely studied in Arctic environments (Pienitz et al. 1992, 2000; Willemse et al. 2004). Continuous desalinization suggests continuously increasing lake size and rising water level together with relatively decreasing material input or reduced leaching of salt-rich solutes from the surrounding sediments. Nevertheless, the major lake water ion source is still likely to be the salt-rich upthrust marine sediments (Kokelj et al. 2002; Fritz et al. 2012b).

A hydrochemical regime shift from marine-derived (Na^+ , Cl^-) to terrestrial-dominated ion composition (Ca^{2+} , Mg^{2+}) is apparent at the hiatus (Fig. 5). While marine-derived ions continued to decrease, terrestrially-derived ions increased sharply at the sedimentary hiatus, together with a slight increase in EC. Ion concentrations remain elevated throughout the pore-water record. XRF-derived sediment geochemistry and pore-water hydrochemistry indicate a strong input and rapid accumulation of terrestrial material leading to the hiatus. This might be derived from active-layer detachments, lake-shore erosion and large slumping events sometime between 1590 and 1040 cal BP. Lenz et al. (2013) suggested an episodic and catastrophic sediment input from the catchment by thermal shoreline erosion based on a sandy layer—coarser material indicates higher transport energy—and a shift in

biogeochemical sediment properties such as low $\delta^{13}\text{C}$ ratios. Sediments originating from disturbance are organic-poor, relatively coarse-grained and show a maximum in Mn/Fe ratio and low Sr/Ca ratios, indicating little authigenic carbonate production. In a graded sequence, fine particles and organic matter deposit last. At the upper end of the disturbed sequence, the decrease in pore-water pH and sharp decrease in Mn/Fe ratio indicates more anaerobic conditions. This conclusion is further supported by good organic-matter preservation. The minimum in HCO_3^- at the uppermost part of the disturbed sequence also suggests elevated bioproductivity and an uptake of HCO_3^- from the lake water, for example by algae which then in turn lowered pH and oxygen availability.

Warmer air temperatures together with higher precipitation or higher runoff would also be an appropriate trigger for more intensive thermokarst processes and sediment mobilization. However, thermokarst is a process that is not solely linked to climate so that this linkage remains speculative. More interesting than a relation to climate might be the geochemical predisposition of the lacustrine system for calcareous organisms.

Autochthonous versus allochthonous deposition of calcareous microfossils

Sediments of unit A older than 11,000 cal BP are composed of thawed upthrust glacial sediments, which have a marine origin on the Beaufort Shelf, as indicated by the presence of marine and marine-brackish foraminifers, ostracods and remains of marine mollusks. The latter are completely missing in the other core sections and harder to transport than microfossils. A comparison of faunal assemblages in unit A with our reference samples shows closest relations to the modern marine and Pleistocene fauna (Fig. 9a). This similarity points to lake expansion in Pleistocene marine material in response to thaw subsidence and with little autochthonous lake sediments. In general, we conclude that increasing similarity with Pleistocene permafrost samples indicates increased reworking of calcareous fossils and allochthonous transport into the lake by thermokarst and shore erosion.

High abundance of freshwater ostracods in the upper units from $\sim 10,000$ cal BP until today

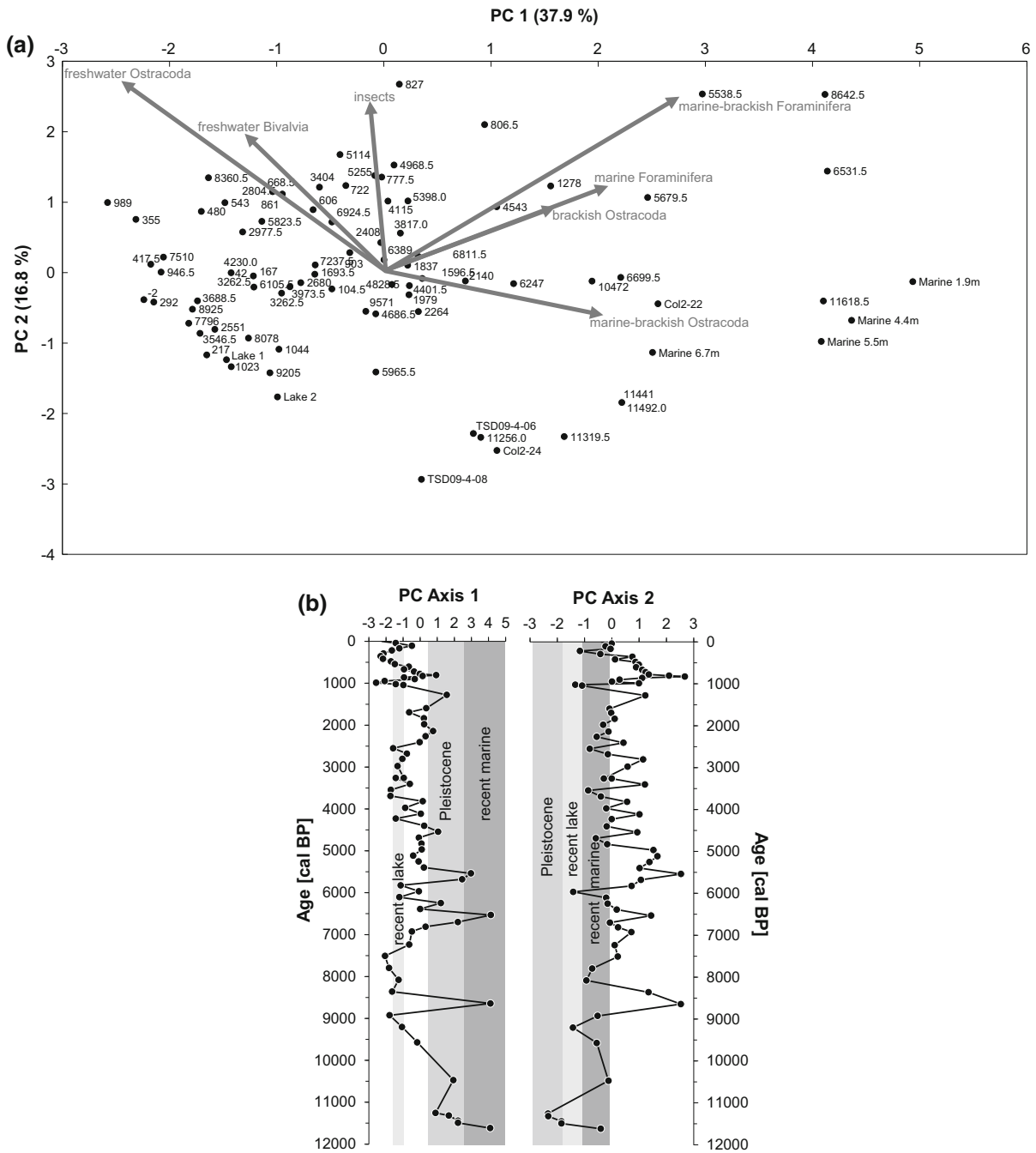


Fig. 9 Principal component analysis (PCA) of fauna assemblages in sediments of Lake Herschel. **a** The first two axes explain 54.7% of the variance. Lake sediment samples from the core are compared to endmembers of recent littoral samples (Lake 1 and 2), recent marine samples (Marine 1.9, 4.4, 5.5 and 6.7 m) and Pleistocene samples in permafrost (Col2-22 and -24

and TSD09-4-06). **b** Samples scores of the first (PC Axis 1) and second axis (PC Axis 2) from fauna assemblages in sediments of Lake Herschel are compared to sample scores to the endmembers of recent lake samples, recent marine samples and Pleistocene samples in permafrost to illustrate similarity and dissimilarity

indicates at least oligohaline conditions (Meisch 2000). The majority of the samples also yield marine to brackish microfossils, sometimes in high numbers. Their coexistence can be explained by erosion of Pleistocene upthrust marine sediments in the catchment, transportation and deposition of easily transportable foraminifers, and, to a lesser degree, of ostracods into the lake basin. There is a general trend towards lower numbers of marine components over time, which can be explained by changing water chemistry towards lower concentrations of marine-derived ions as indicated by the pore-water record. Based on the similarity between core-based microfossils and marine and Pleistocene marine reference samples, reworking phases are most prominent between 8700 and 8300 cal BP, 6900 and 5300 cal BP, and at the hiatus between 1590 and 1040 cal BP (Fig. 9b), due to higher allochthonous input from the catchment. Stronger geomorphic disturbance due to thermokarst, and possibly higher precipitation and runoff are considered to be the most likely reasons. As the brackish microfossils are abundant and partly well-preserved, we cannot exclude the possibility that some of the brackish taxa actually lived in the lake if its water chemistry was oligohaline to mesohaline and relatively stable. Athalassic foraminifera and ostracod faunas are a common phenomenon in inland salt-water bodies (De Deckker 1981; Pint et al. 2012); therefore the presence of brackish foraminifers or ostracods in Lake Herschel would not be surprising. The short distance to the sea would make an avian-mediated introduction of marginal marine taxa easy, as long as lake-water salinity was high enough and relatively stable. Modern and Pleistocene marine reference samples show a trend towards lower similarity with the core over time (Fig. 9b). This trend might reflect stabilizing surface conditions around the lake towards the late Holocene; with the exception of the event being responsible for the hiatus.

The lower proportion of freshwater taxa at the hiatus suggests higher mobilization of permafrost-derived marine and brackish taxa. Thereafter, the lake stabilized and freshwater taxa, especially ostracods, occurred steadily and in relatively high numbers. Plant fragments including submersed taxa such as *Potamogeton* were frequent in sediments covering the last 1000 years pointing to higher productivity and good preservation conditions. Higher productivity could have been caused by higher temperatures and less

saline water conditions. Improved organic-matter preservation may also have occurred under anaerobic conditions and at episodes of rapid sedimentation and burial. Neither the calcareous microfossil record nor the XRF geochemical record showed any significant reaction to major Holocene climate fluctuations like the 8.2 ka event (Alley and Ágústsdóttir 2005), the 4.2 ka event (Booth et al. 2005) or the 2.8 ka event (van Geel et al. 2014), indicated as blue marker lines in Figs. 3 and 4. We therefore suggest that episodic thermokarst processes and changes in lake-water properties are the main drivers of ecosystem change, calcareous microfossil assemblages and geochemical processes in the lake catchment.

Regional pollen-based reconstruction of vegetation and climate

Our pollen-based climate record does not match well with other summer air temperature reconstructions from the region (Viau et al. 2008; Bunbury and Gajewski 2009; Kurek et al. 2009; Viau and Gajewski 2009; Fritz et al. 2012a; Irvine et al. 2012; Gajewski 2015a). This may be due to a couple of factors. The value of the squared chord distance in the reconstruction is rather high (Fig. 8; Gajewski 2015a) so the fossil samples from the Herschel core do not find good analogues in the modern dataset (Whitmore et al. 2005). The typical modern vegetation on Herschel Island consists of sedges, mosses and erect dwarf shrubs or low shrubs (CAVM Team 2003), and these conditions may not be well represented in the modern dataset.

Even during the Holocene, the mediating effect of sea-level rise on summer air temperatures seems to have changed the local climate very little. In contrast to other locations at the Arctic Ocean facing a broad and shallow shelf, Herschel Island is located close to the steep slopes of the Mackenzie Trough directly north of the island. As pointed out by Fritz et al. (2012b), the distance to the sea was not much farther than today, even at times of low sea level at the early phases of the Holocene.

Obu et al. (2017) and Wolter et al. (2016) have shown that vegetation on Herschel Island is closely related to periglacial surface morphology and sub-surface conditions, which cover a very broad range on the high-relief island. Wolter et al. (2016, 2017) demonstrated that even small-scale vegetation

patterns vary within a single ecological unit such as polygonal wetlands, depending on active-layer thickness and soil temperatures. The lake is surrounded by ice-wedge polygons that are dominated by Cyperaceae. This may help explain the relatively large values of Cyperaceae in the pollen spectrum, which points to wet and cool climate conditions. Fritz et al. (2016) have used the Cyperaceae/Poaceae ratio from a peat core in ice-wedge polygon terrain on Herschel Island as an indicator of wetland development on the local scale rather than climate variation. However, high Cyperaceae values are also indicative of middle-Arctic conditions and Poaceae percentages are greater in High-Arctic pollen assemblages (Gajewski 2002). The mixing of a temperature and moisture signal may be contributing to the muted variation in the reconstruction.

Pollen concentrations and influx were higher during the past 5500 years when the climate reconstruction indicates lower values of July temperature (Fig. 8), again contrary to the usual pattern in Arctic pollen diagrams (Gajewski 2015b). This suggests that pollen input to the sediment is likely controlled more by sedimentation patterns within the lake than due to pollen production in the catchment. The cooler temperatures in the late Holocene are in good agreement with a reconstruction of July temperatures based on pollen records from Banks, Victoria and Melville Island (Gajewski 2015a), in both cases showing an abrupt cooling that started between 4000 and 3500 cal BP.

Conclusions

Athalassic subsaline lakes, such as Lake Herschel (Yukon, Canada), have been rarely studied in Arctic environments. Geochemical, hydrochemical, and paleoecological investigations of lake sediments in a thermokarst setting provided environmental conditions reconstructed on a local to regional scale. Episodic permafrost disturbance in the catchment has been a predominant influence on the sedimentological record of such thermokarst lakes. Apart from being a precise climate archive, thermokarst lake sediment records provide valuable information on local/regional changes in sediment transport, hydrology, nutrient availability and surface disturbance, which might relate to climatic variation.

This study has shown that the inc/coh ratio of XRF core scans provide a high-resolution semi-quantitative organic carbon proxy record that correlates well with TOC measurements performed at coarser resolution. XRF-derived Mn/Fe ratios are a robust indicator of aerobic versus anaerobic conditions that moderate the preservation potential of organic matter in lake sediments. Continuous desalinization is indicated by pore-water hydrochemistry and the XRF-derived Sr/Ca ratio. This implies increasing lake size and lake level together with a relatively decreasing input of solute-rich material. The chemical composition of catchment sediments provides a predisposition for the living conditions of calcareous microfaunal communities in Lake Herschel. Elevated salinity allows the establishment of brackish taxa in an athalassic setting. The onset of the lacustrine sequence was characterized by reworking of older marine sediments and their associated microfauna as well as saline conditions that provided a habitat for autochthonous brackish ostracods and foraminifers. Intermittent similarities with reference samples from Pleistocene permafrost and low numbers of freshwater taxa indicate reworking phases of calcareous fossils and allochthonous transport into the lake by active thermokarst processes and shore erosion.

Quantitative climate reconstructions based on pollen are not recommended for thermokarst lakes with actively eroding shore lines and small catchments. First, older pollen might be reworked from catchment sediments and reworking might not be clearly recognized due to short transport pathways. Second, small catchments may lead to an over-representation of local vegetation in the pollen assemblage, which is not solely related to climate but to permafrost conditions regulating microtopography, nutrient availability and moisture regime.

With this multidisciplinary study, we have shown that thermokarst lake sediments represent a valuable environmental archive and that such aquatic ecosystems are extremely vulnerable to disturbances in the catchment. Projected permafrost thaw in the future will increase the lateral material transport into aquatic ecosystem, thus making thermokarst lakes an important net sink and location for carbon and nutrient turnover in terrestrial Arctic environments.

Acknowledgements We wish to express our thanks to the Yukon Territorial Government and the Yukon Parks (Herschel

Island Qiqiktaruk Territorial Park). The authors acknowledge the support of the Aurora Research Institute (ARI, Inuvik) for the field component. This study was partly funded by the German Federal Ministry of Education and Research (BMBF Grant No. CAN 09/001, 01DM12002), the German Science Foundation (DFG Grant No. LA 2399/3-1), the Helmholtz Association (Grant No. VH-NG-801), a dissertation stipend by the Potsdam University and a fellowship by the Association for Canadian Studies awarded to JL, and by a fellowship awarded to MF by the German Federal Environmental Foundation (DBU) (Grant No. 20008/953) and the Daimler and Benz Foundation (Grant No. 32-02/15). KG and NP were supported by a Discovery Grant from the Natural Sciences and Engineering Research Council of Canada (NSERC). The study contributes to the *Arctic Ecological Network* (Arc-EcoNet) funded by the BMBF (Grant No. 01DJ14003). Field support was provided by Boris Radosavljevic, Gerald Müller, Gregory De Pascale, and Samuel McLeod. Analytical support was provided by Lutz Schirmer (AWI) for modern marine ostracods, by Antje Eulenburg (AWI) with hydrochemical analyses and by Volker Wennrich and Sonja Berg (University of Cologne, Germany) with XRF scanning.

References

- Alley RB (2000) The Younger Dryas cold interval as viewed from central Greenland. *Quat Sci Rev* 19:213–226
- Alley RB, Ágústsdóttir AM (2005) The 8k event: cause and consequences of a major Holocene abrupt climate change. *Quat Sci Rev* 24:1123–1149
- Booth RK, Jackson ST, Forman SL, Kutzbach JE, Bettis EA III, Kreigs J, Wright DK (2005) A severe centennial-scale drought in midcontinental North America 4200 years ago and apparent global linkages. *Holocene* 15:321–328
- Bronk Ramsey C (2008) Deposition models for chronological records. *Quat Sci Rev* 27:42–60
- Bronk Ramsey C (2009a) Bayesian analysis of radiocarbon dates. *Radiocarbon* 51:337–360
- Bronk Ramsey C (2009b) Dealing with outliers and offsets in radiocarbon dating. *Radiocarbon* 51:1023–1045
- Bunbury J, Gajewski K (2009) Postglacial climates inferred from a lake at treeline, southwest Yukon Territory, Canada. *Quat Sci Rev* 28:354–369
- Burn CR (1997) Cryostratigraphy, paleogeography, and climate change during the early Holocene warm interval, western Arctic coast, Canada. *Can J Earth Sci* 34:912–925
- Burn CR, Smith MW (1990) Development of thermokarst lakes during the Holocene at sites near Mayo, Yukon Territory. *Permafrost Periglacial* 1:161–175
- Burn CR, Michel FA, Smith MW (1986) Stratigraphic, isotopic, and mineralogical evidence for an early Holocene thaw unconformity at Mayo, Yukon Territory. *Can J Earth Sci* 23:79–803
- Burnett AP, Soreghan MJ, Scholz CA, Brown ET (2011) Tropical East African climate change and its relation to global climate: a record from Lake Tanganyika, Tropical East Africa, over the past 90 + kyr. *Palaeogeogr Palaeoclimatol Palaeoecol* 303:155–167
- CAVM Team (2003) Circumpolar Arctic vegetation map. (1:7,500,000 scale), Conservation of Arctic Flora and Fauna (CAFF) map no. 1, U.S. Fish and Wildlife Service, Anchorage, Alaska
- Chawchai S, Kylander ME, Chabangborn A, Löwemark L, Wohlfarth B (2016) Testing commonly used X-ray fluorescence core scanning-based proxies for organic-rich lake sediments and peat. *Boreas* 45:180–189
- Cohen AS (2003) *Paleolimnology: the history and evolution of lake systems*. Oxford University Press, New York, p 500
- Croudace IW, Rindby A, Rothwell RG (2006) ITRAX: description and evaluation of a new multi-function X-ray core scanner. *Geol Soc Lond Spec Publ* 267:51–63
- Cwynar LC (1982) A late-quaternary vegetation history from Hanging Lake, northern Yukon. *Ecol Monogr* 52:1–24
- Cwynar LC, Spear RW (1991) Reversion of forest to tundra in the central Yukon. *Ecology* 72:202–212
- Dallimore A, Schröder-Adams CJ, Dallimore SR (2000) Holocene environmental history of thermokarst lakes on Richards Island, Northwest Territories, Canada: the-camoebians as paleolimnological indicators. *J Paleolimnol* 23:261–283
- De Deckker P (1981) 10. Ostracods of athalassic saline lakes. *Hydrobiologia* 81–82:131–144
- Dutta K, Schuur EAG, Neff JC, Zimov SA (2006) Potential carbon release from permafrost soils of Northeastern Siberia. *Glob Change Biol* 12:2336–2351
- Engstrom DR, Wright HE Jr (1984) Chemical stratigraphy of lake sediments as a record of environmental change. In: Haworth EY, Lund JWG (eds) *Lake sediments and environmental history: studies in palaeolimnology and palaeoecology in honour of Winifred Tutin*. Leicester University Press, Leicester, p 411
- Environment Canada (2015). http://climate.weather.gc.ca/index_e.html. Accessed October 2015
- Fritz M, Wetterich S, Meyer H, Schirmer L, Lantuit H, Pollard WH (2011) Origin and characteristics of massive ground ice on Herschel Island (western Canadian Arctic) as revealed by stable water isotope and hydrochemical signatures. *Permafrost Periglacial* 22:26–38
- Fritz M, Herzschuh U, Wetterich S, Lantuit H, De Pascale GP, Pollard WH, Schirmer L (2012a) Late glacial and Holocene sedimentation, vegetation, and climate history from easternmost Beringia (northern Yukon Territory, Canada). *Quat Res* 78:549–560
- Fritz M, Wetterich S, Schirmer L, Meyer H, Lantuit H, Preusser F, Pollard WH (2012b) Eastern Beringia and beyond: late Wisconsinan and Holocene landscape dynamics along the Yukon Coastal Plain, Canada. *Palaeogeogr Palaeoclimatol* 319–320:28–45
- Fritz M, Wolter J, Rudaya N, Palagushkina O, Nazarova L, Obu J, Rethemeyer J, Lantuit H, Wetterich S (2016) Holocene ice-wedge polygon development in northern Yukon permafrost peatlands (Canada). *Quat Sci Rev* 147:279–297
- Fritz M, Unkel I, Lenz J, Gajewski K, Frenzel P, Paquette N, Lantuit H, Körte L, Wetterich S (2018) Radiocarbon dates, porewater hydrochemistry, calcareous microfossils and pollen data from a lake sediment core (PG1967) from Herschel Island (Yukon, Canada). *PANGAEA*. <https://doi.pangaea.de/10.1594/PANGAEA.886875>

- Gajewski K (2002) Modern pollen assemblages in lake sediments from the Canadian Arctic. *Arct Antarct Alp Res* 34:26–32
- Gajewski K (2015a) Quantitative reconstruction of Holocene temperatures across the Canadian Arctic and Greenland. *Glob Planet Change* 128:14–23
- Gajewski K (2015b) Impact of Holocene climate variability on Arctic vegetation. *Glob Planet Change* 133:272–287
- Grosse G, Schirmer L, Kunitsky VV, Hubberten H-W (2005) The use of CORONA images in remote sensing of periglacial geomorphology: an illustration from the NE Siberian coast. *Permafrost Periglacial* 16:163–172
- Guyard H, Chapron E, St-Onge G, Anselmetti FS, Arnaud F, Magand O, Francus P, Mélières M-A (2007) High-altitude varve records of abrupt environmental changes and mining activity over the last 4000 years in the western French Alps (Lake Bramant, Grandes Rousses Massif). *Quat Sci Rev* 26:2644–2660
- Hammer Ø, Harper DAT, Ryan PD (2001) PAST: paleontological statistics software package for education and data analysis. *Palaeontol Electron* 4:1–9
- Hinkel KM, Eisner WR, Bockheim JG, Nelson FE, Peterson KM, Dai X (2003) Spatial extent, age, and carbon stocks in drained thaw lake basins on the Barrow Peninsula, Alaska. *Arct Antarct Alp Res* 35:291–300
- Hinkel KM, Frohn RC, Nelson FE, Eisner WR, Beck RA (2005) Morphometric and spatial analysis of thaw lakes and drained thaw lake basins in the western Arctic Coastal Plain, Alaska. *Permafrost Periglacial* 16:327–341
- Irvine F, Cwynar L, Vermaire J, Rees AH (2012) Midge-inferred temperature reconstructions and vegetation change over the last ~ 15,000 years from Trout Lake, northern Yukon Territory, eastern Beringia. *J Paleolimnol* 48:133–146
- Jin Z, Wang S, Shen J, Zhang E, Li F, Ji J, Lu X (2001) Chemical weathering since the Little Ice Age recorded in lake sediments: a high-resolution proxy of past climate. *Earth Surf Proc Land* 26:775–782
- Jones BM, Arp CD (2015) Observing a catastrophic thermokarst lake drainage in northern Alaska. *Permafrost Periglacial* 26:119–128
- Kaufman DS, Manley WF (2004) Pleistocene maximum and late Wisconsinan glacier extents across Alaska, U.S.A. In: Ehlers J, Gibbard PL (eds) *Quaternary glaciations—extent and chronology, part II: North America*. Elsevier, Amsterdam, pp 9–27
- Kaufman DS, Ager TA, Anderson NJ, Anderson PM, Andrews JT, Bartlein PJ, Brubaker LB, Coats LL, Cwynar LC, Duvall ML, Dyke AS, Edwards ME, Eisner WR, Gajewski K, Geirsdottir A, Hu FS, Jennings AE, Kaplan MR, Kerwin MW, Lozhkin AV, MacDonald GM, Miller GH, Mock CJ, Oswald WW, Otto-Bliesner BL, Porinchu DF, Ruhland K, Smol JP, Steig EJ, Wolfe BB (2004) Holocene thermal maximum in the western Arctic (0–180°W). *Quat Sci Rev* 23:529–560
- Kaufman DS, Axford YL, Henderson ACG, McKay NP, Oswald WW, Saenger C, Anderson RS, Bailey HL, Clegg B, Gajewski K, Hu FS, Jones MC, Massa C, Routson CC, Werner Wooller MJ, Yu ZC (2016) Holocene climate changes in eastern Beringia (NW North America)—a systematic review of multi-proxy evidence. *Quat Sci Rev* 147:312–339
- Koinig K, Shotyk W, Lotter A, Ohlendorf C, Sturm M (2003) 9000 years of geochemical evolution of lithogenic major and trace elements in the sediment of an alpine lake—the role of climate, vegetation, and land-use history. *J Paleolimnol* 4:307–320
- Kokelj SV, Smith CAS, Burn CR (2002) Physical and chemical characteristics of the active layer and permafrost, Herschel Island, western Arctic Coast, Canada. *Permafrost Periglacial* 13:171–185
- Koven CD, Ringeval B, Friedlingstein P, Ciais P, Cadule P, Khvorostyanov D, Krinner G, Tarnocai C (2011) Permafrost carbon-climate feedbacks accelerate global warming. *Proc Natl Acad Sci USA* 108:14769–14774
- Kurek J, Cwynar LC, Vermaire JC (2009) A late Quaternary paleotemperature record from Hanging Lake, northern Yukon Territory, eastern Beringia. *Quat Res* 72:246–257
- Lenz J, Fritz M, Schirmer L, Lantuit H, Wooller MJ, Pollard WH, Wetterich S (2013) Periglacial landscape dynamics in the western Canadian Arctic: results from a thermokarst lake record on a push moraine (Herschel Island, Yukon Territory). *Palaeogeogr Palaeoclimatol* 381–382:15–25
- Lenz J, Jones BM, Wetterich S, Tjallingii R, Fritz M, Arp CD, Rudaya N, Grosse G (2016) Impacts of shore expansion and catchment characteristics on lacustrine thermokarst records in permafrost lowlands. *Alsk Arctic Coast Plain Arktos* 2:25
- Löwemark L, Chen H-F, Yang T-N, Kylander M, Yu E-F, Hsu Y-W, Lee T-Q, Song S-R, Jarvis S (2011) Normalizing XRF-scanner data: a cautionary note on the interpretation of high-resolution records from organic-rich lakes. *J Asian Earth Sci* 40:1250–1256
- Mackay JR (1959) Glacier ice-thrust features of the Yukon Coast. *Geogr Bull* 13:5–21
- Mackay JR (1988) Catastrophic lake drainage, Tuktoyaktuk Peninsula area, District of Mackenzie. Current research part D: interior plains and Arctic Canada, Geological Survey of Canada paper no. 88-1D:83-90
- Marsh P, Russell M, Pohl S, Haywood H, Onclin C (2009) Changes in thaw lake drainage in the Western Canadian Arctic from 1950 to 2000. *Hydrological Process* 23:145–158
- Meisch C (2000) Freshwater Ostracoda of western and central Europe. In: Schwoerbel J, Zwick P (eds) *Stüßwasserfauna von Mitteleuropa* 8/3. Spektrum Akademischer Verlag, Heidelberg, p 522
- Mischke S, Kramer M, Zhang C, Shang H, Herzsich U, Erzinger J (2008) Reduced early Holocene moisture availability in the Bayan Har Mountains, northeastern Tibetan Plateau, inferred from a multi-proxy lake record. *Palaeogeogr Palaeoclimatol* 26:59–76
- Mook WG, van der Plicht J (1999) Reporting ^{14}C activities and concentrations. *Radiocarbon* 41:227–239
- Murton JB (2001) Thermokarst sediments and sedimentary structures, Tuktoyaktuk Coastlands, western Arctic Canada. *Glob Planet Change* 28:175–192
- Obu J, Lantuit H, Myers-Smith I, Heim B, Wolter J, Fritz M (2017) Effect of terrain characteristics on soil organic carbon and total nitrogen stocks in soils of Herschel Island, western Canadian Arctic. *Permafrost Periglacial* 28:92–107

- Pienitz R, Walker IR, Zeeb BA, Smol JP, Leavitt PR (1992) Biomonitoring past salinity changes in an athalassic subarctic lake. *Int J Salt Lake Res* 1:91–123
- Pienitz R, Smol JP, Last WM, Leavitt PR, Cumming BF (2000) Multi-proxy Holocene paleoclimatic record from a saline lake in the Canadian Subarctic. *Holocene* 10:673–686
- Pint A, Frenzel P, Fuhrmann R, Scharf B, Wennrich V (2012) Distribution of *Cyprideis torosa* (Ostracoda) in Quaternary athalassic sediments in Germany and its application for palaeoecological reconstructions. *Int Rev Hydrobiol* 97:330–355
- R Core Team (2014) R: a language and environment for statistical computing. R Foundation for Statistical Computing, Vienna, Austria. <http://www.R-project.org/>. Accessed 10 Dec 2015
- Rampton VN (1988) Quaternary geology of the Tuktoyaktuk coastlands, Northwest Territories. *Memoir* 423
- Reimer PJ, Bard E, Bayliss A, Beck JW, Blackwell PG, Bronk Ramsey C, Buck CE, Cheng H, Edwards RL, Friedrich M, Grootes PM, Guilderson TP, Haflidason H, Hajdas I, Hatté C, Heaton TJ, Hoffmann DL, Hogg AG, Hughen KA, Kaiser KF, Kromer B, Manning SW, Niu M, Reimer RW, Richards DA, Scott EM, Southon JR, Staff RA, Turney CSM, van der Plicht J (2013) IntCal13 and marine13 radiocarbon age calibration curves 0–50,000 years cal BP. *Radiocarbon* 55:1869–1887
- Ricketts RD, Johnson TC, Brown ET, Rasmussen KA, Romanovsky VV (2001) The Holocene paleolimnology of Lake Issyk-Kul, Kyrgyzstan: trace element and stable isotope composition of ostracodes. *Palaeogeogr Palaeoclimatol* 176:207–227
- Ritchie JC, Cwynar LC, Spear RW (1983) Evidence from northwest Canada for an early Holocene Milankovitch thermal maximum. *Nature* 305:126–128
- Röhl U, Abrams LJ (2000) High-resolution, downhole, and nondestructive core measurements from Site 999 and 1001 in the Caribbean Sea: application to the Late Paleocene Thermal Maximum. *Proc Ocean Drill Program Sci Results* 165:191–203
- Schaefer K, Lantuit H, Romanovsky VE, Schuur EAG, Witt W (2014) The impact of the permafrost carbon feedback on global climate. *Environ Res Lett* 9:085003
- Smith CAS, Kennedy CL, Hargrave AE, McKenna KM (1989) Soil and vegetation of Herschel Island. Yukon Soil Survey Report No.1, LRRC Contribution No. 88–26, Agriculture Canada, Whitehorse, Yukon, p 101
- Spear RW (1993) The palynological record of Late-Quaternary arctic tree-line in northwest Canada. *Rev Palaeobot Palynol* 79:99–111
- Tjallingii R, Röhl U, Kölling M, Bickert T (2007) Influence of the water content on X-ray fluorescence core-scanning measurements in soft marine sediments. *Geochem Geophys Geosyst* 8:Q02004
- van Geel B, Heijnis H, Charman DJ, Thompson G, Engels S (2014) Bog burst in the eastern Netherlands triggered by the 2.8 kyr BP climate event. *Holocene* 24:1465–1477
- van Huissteden J, Berrittella C, Parmentier FJW, Mi Y, Maximov TC, Dolman AJ (2011) Methane emissions from permafrost thaw lakes limited by lake drainage. *Nat Clim Change* 1:119–123
- Viau AE, Gajewski K (2009) Reconstructing millennial-scale, regional paleoclimates of boreal Canada during the Holocene. *J Clim* 22:316–330
- Viau AE, Gajewski K, Sawada MC, Bunbury J (2008) Low- and high-frequency climate variability in eastern Beringia during the past 25000 years. *Can J Earth Sci* 45:1435–1453
- Wahl HE, Fraser DB, Harvey RC, Maxwell JB (1987) Climate of Yukon. *Environ Can Atmos Environ Serv Climatol Stud* 40:1–323
- Walter Anthony KM, Zimov SA, Grosse G, Jones MC, Anthony PM, Chapin FS III, Finlay JC, Mack MC, Davydov S, Frenzel P, Frolking S (2014) A shift of thermokarst lakes from carbon sources to sinks during the Holocene epoch. *Nature* 511:452–456
- Weltje GJ, Tjallingii R (2008) Calibration of XRF core scanners for quantitative geochemical logging of sediment cores: theory and application. *Earth Planet Sci Lett* 274:423–438
- Whitmore J, Gajewski K, Sawada M, Williams JW, Shuman B, Bartlein PJ, Minckley T, Viau AE, Webb T III, Shafer S, Anderson P, Brubaker L (2005) Modern pollen data from North America and Greenland for multi-scale paleoenvironmental applications. *Quat Sci Rev* 24:1828–1848
- Willemse N, van Dam O, van Helvoort P-J, Dankers R, Brommer M, Schokker J, Valstar T, de Wolf H (2004) Physical and chemical limnology of a subsaline athalassic lake in west Greenland. *Hydrobiologia* 524:167–192
- Williams JW, Shuman B, Bartlein PJ, Whitmore J, Gajewski K, Sawada M, Minckley T, Shafer S, Viau AE, Webb T III, Anderson PM, Brubaker LB, Whitlock C, Davis OK (2006) An atlas of pollen-vegetation-climate relationships for the United States and Canada. American Association of Stratigraphic Palynologists Foundation, Dallas, p 293
- Wolter J, Lantuit H, Fritz M, Macias-Fauria M, Myers-Smith I, Herzschuh U (2016) Vegetation composition and shrub extent on the Yukon coast, Canada, are strongly linked to ice-wedge polygon degradation. *Polar Res* 35:27489
- Wolter J, Lantuit H, Herzschuh U, Stettner S, Fritz M (2017) Tundra vegetation stability versus lake-basin variability on the Yukon Coastal Plain (NW Canada) during the past three centuries. *Holocene* 27:1846–1858
- Zabenskie S, Gajewski K (2007) Post-glacial climatic change on Boothia Peninsula, Nunavut, Canada. *Quat Res* 68:261–270
- Zabenskie S, Peros M, Gajewski K (2006) The use of heavy-liquid in the separation of pollen from Arctic lake sediments. *Can Assoc Palynol Newslett* 29:5–7
- Zazula GD, Hare PG, Storer JE (2009) New radiocarbon-dated vertebrate fossils from Herschel Island: implications for the palaeoenvironments and glacial chronology of the Beaufort Sea coastlands. *Arctic* 62:273–280